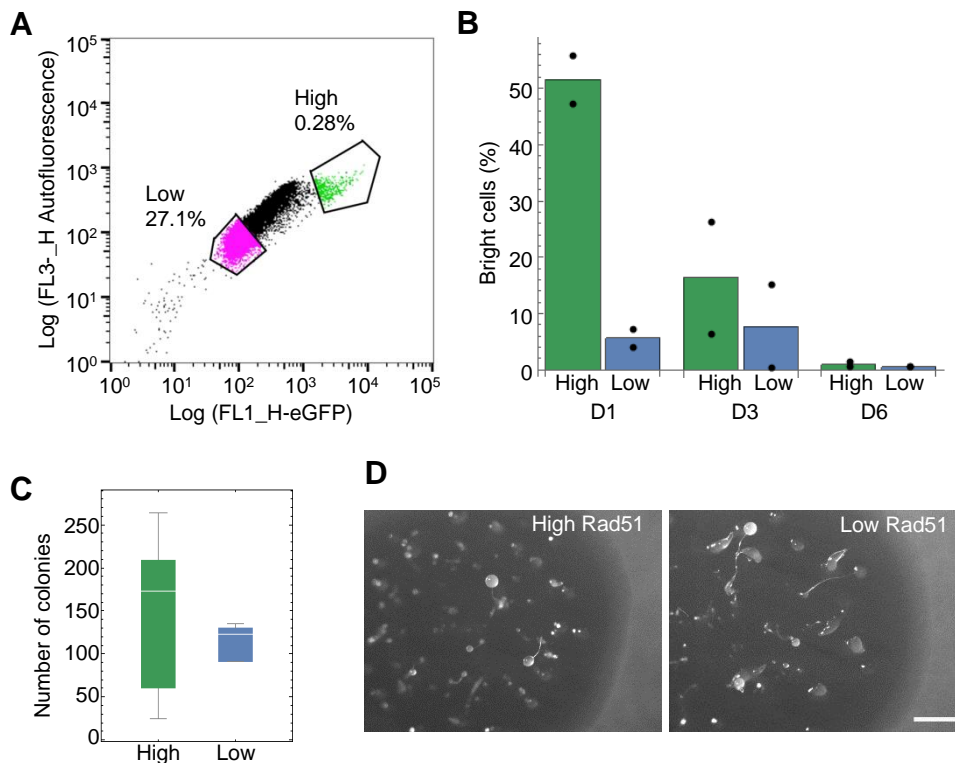


**Fig. S1. Rad51-Neon as a marker for spontaneous DNA damage.**

(A) Immuno-staining of Rad51-Neon cells with antibody against phosphorylated histone H2AX, which gives an enriched signal in cells undergoing DNA damage. Cells were not treated with any DNA damaging agents, so antibody staining marks out cells that have suffered spontaneous damage. Scale bar is 20  $\mu$ m. (B) Correlations between phosphorylated histone H2AX staining and Rad51-Neon levels. These plots are two experimental repeats of the plot in Fig. 2A. Left:  $r=0.49$ ,  $p=8.2 \times 10^{-27}$ ; right:  $r=0.81$ ,  $p=3.6 \times 10^{-88}$ . (C) Variability of GO annotated DNA repair genes in undifferentiated Dictyostelium cells. Plot shows the relationship between mean expression (read counts) and variability ( $CV^2$  – the squared coefficient of variation) for individual genes. Each gene is represented as a dot, with the red line showing a running median through the cloud of points. DNA repair genes shown in black. Genes above the line are more variable than average, and genes below the line are less variable than average. Data from Antolovic et al. (2017). (D) Flow cytometry data showing the scaling of bleomycin dose to induction of Rad51-Neon expression (one of two biological replicates shown).



**Fig. S2. Long term monitoring of Rad51 expression and the effects of spontaneous DNA damage on cell viability.**

(A) Plot showing the population fractions isolated by FACS for measuring clone forming potential and long-term developmental prognosis. (B) Dynamics of the proportion of high cells, 1 day, 3 days and 6 days after purification of high and low cells by FACS. Cells were assigned to high or low Rad51 using fluorescence microscopy. The low cells show a temporary induction in a small proportion of the population after FACS. Black dots represent values from each of 2 replicates. To assign cells to high or low, an intensity threshold was imposed by eye on a non-sorted population of 2569 Rad51-Neon cells, with the imposed threshold categorising the percentage of bright cells as 0.93%. (C) Clone forming potential of high and low Rad51-Neon cells. Data shows the number of clones recovered, on bacterial growth plates of 150 FACS-sorted high and low Rad51-Neon cells. Data are combined from 5 independent experiments ( $p=0.68$ ). (D) Example images from the 5 biological replicates showing long term developmental potential of single cell clones derived from high and low Rad51 cells is similar.

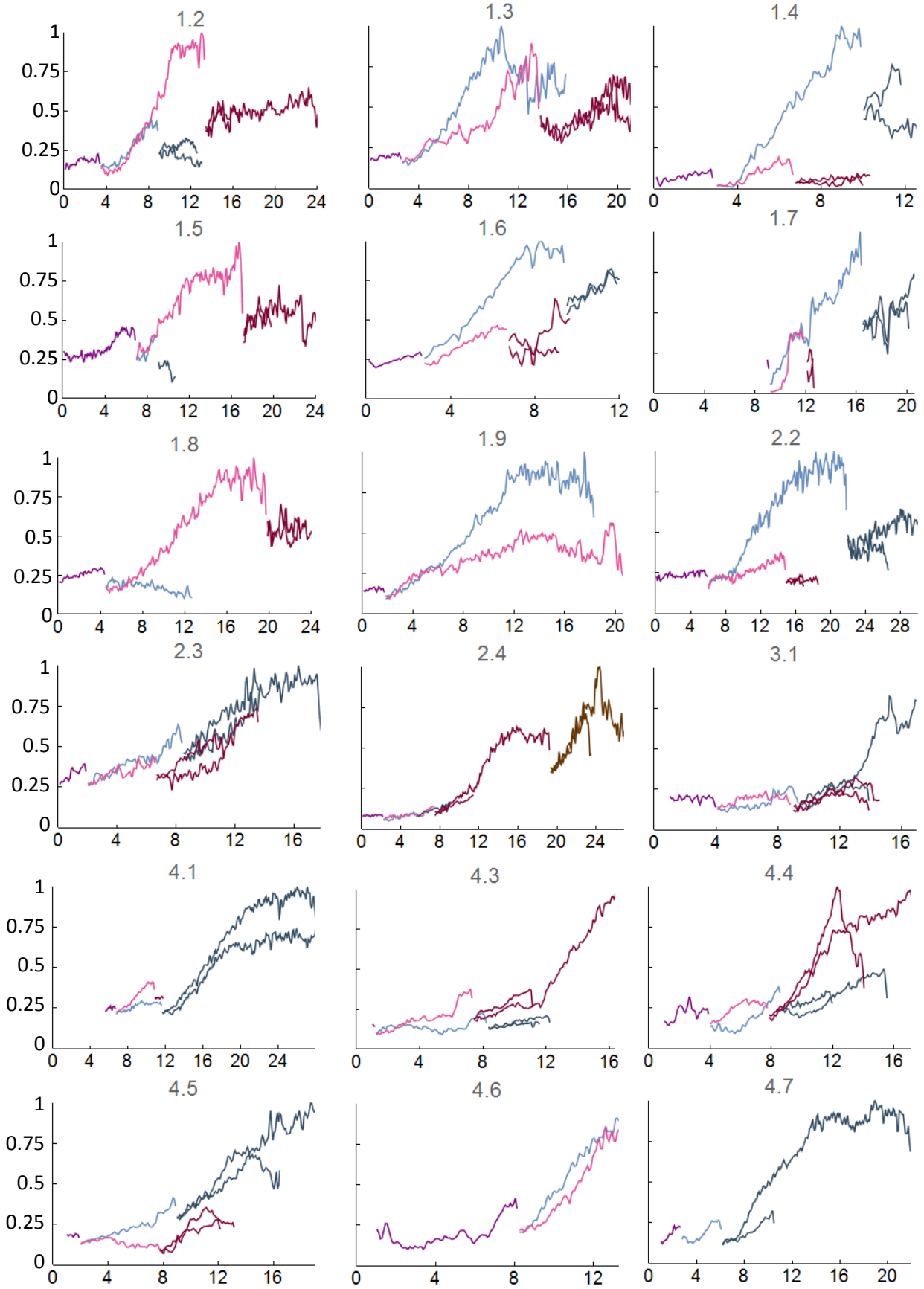


**Fig. S3. Time lapse imaging of spontaneous Rad51-Neon induction.**

Individual panels show intergenerational Rad51 expression dynamics for 18 cell lineages where the complete process of induction was captured from multi-generation time lapse movies of several thousands of cells over 4 independent imaging experiments. This is the expanded dataset relating to Fig. 2D.

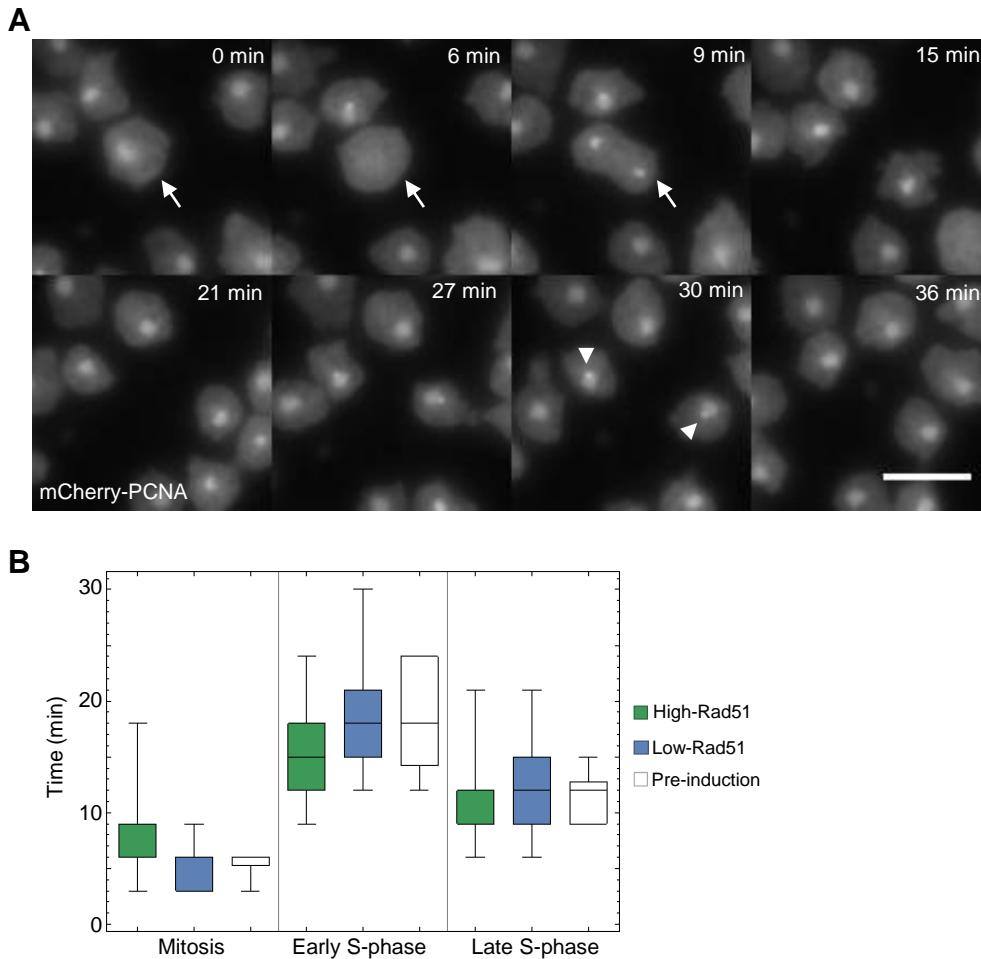


### Fig. S4. Delineating cell cycle phases using mCherry-PCNA.

(A) Upon mitotic entry, nuclear PCNA is dispersed throughout the cell (6 min), before rapidly being recruited back to chromatin upon the onset of division (arrows: 0, 6 and 9 min). There is no G1, with cells immediately commencing early S-phase. The end of early S-phase and the beginning of late S-phase are marked with the appearance of large PCNA foci corresponding to the replication of heterochromatin (arrowheads, 30 min). Scale bar 15  $\mu$ m. (B) The plot shows the durations of the various cell cycle phases for high and low Rad51-Neon cells, and cells prior to Rad51 induction (“pre-induction”), with data pooled from 4 independent replicates. High cells have slightly longer mitoses ( $p=0.0013$ ,  $n=36$  (high) and  $n=57$  (low)), slightly shorter early S-phases ( $p<0.0001$ ,  $n=65$  (high) and  $n=108$  (low)) and no significant change in their late S-phase durations ( $p=0.073$ ,  $n=64$  (high) and  $n=104$  (low)). The rare cells ( $n=5$ ) that could be tracked for their entire cell cycle before Rad51-Neon induction (pre-induction) showed no clear perturbation of M and S-phase durations.

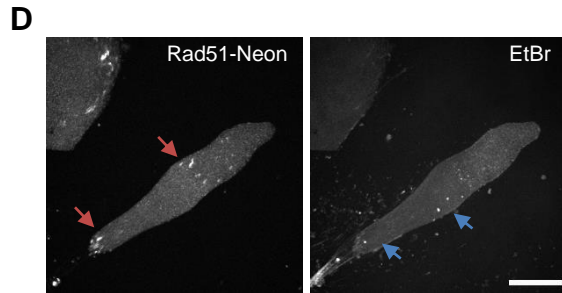
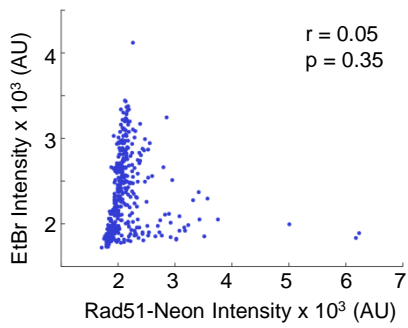
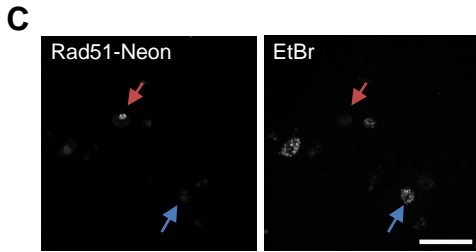
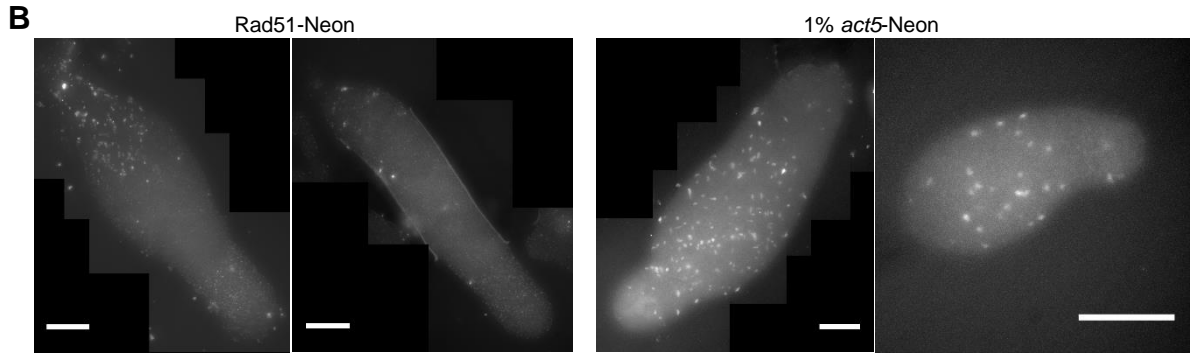
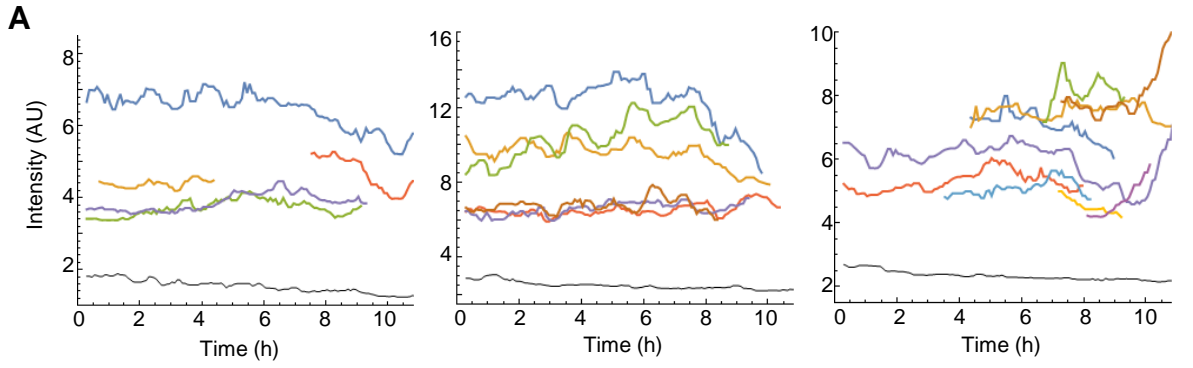


**Fig. S5. Developmental fates of cells undergoing DNA damage.**

(A) No large scale expression changes of high Rad51-Neon cells during early development. Examples of intensity fluctuations of Rad51-Neon during pre-aggregative development. Lines show intensity traces of individual developing Rad51-Neon cells, smoothed with a running median of 6 frames (30 minutes). Cells were tracked until they reached multicellular structures, at which point the fluorescence increased due to convolution effects. The black line at the bottom of the plot shows the fluctuations of the background signal, taken from an area of the field of view without cells. Each plot is a different field-of-view. No strong increases were observed post starvation onset in 6 independent replicates. (B) Examples of slugs generated during development of Rad51-Neon cells (left) and control mixes, with wild-type cells spiked with 1% *act5*-Neon cells (right). Scale bars are 100  $\mu\text{m}$ . Relates to Fig. 4A-C. (C,D) High Rad51-Neon cells do not become Sentinel cells. (C) Staining of cells from disaggregated slugs with ethidium bromide (which labels Sentinel cells), with the plot showing no correlation between Rad51-Neon and ethidium bromide staining ( $r=0.05$ ,  $p=0.35$ ). Typical data from 3 independent experiments. (D) A comparison of ethidium bromide staining and Rad51-Neon in intact slugs. Typical data from 3 independent experiments.

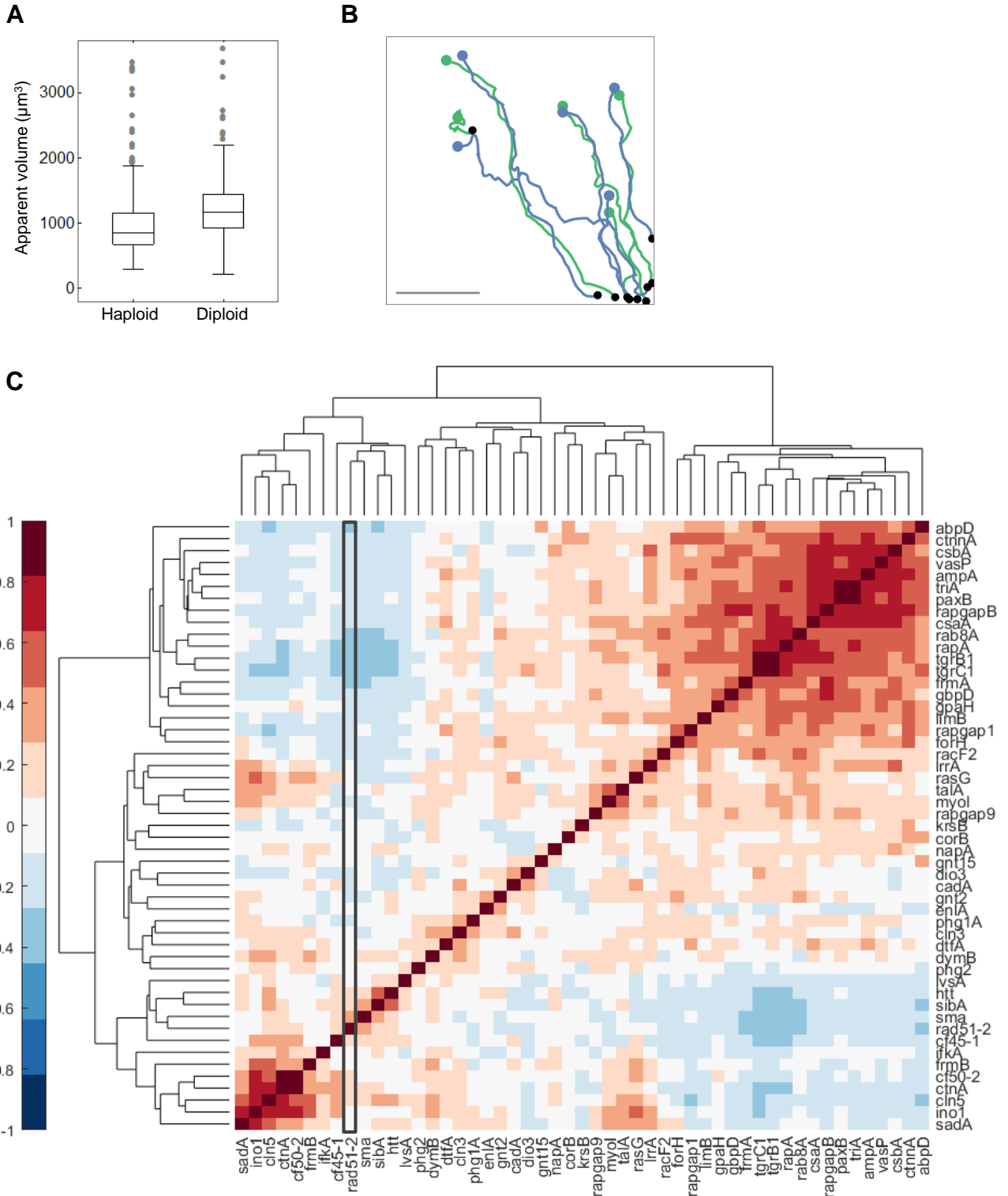


**Fig. S6. Measuring cell size, motility and adhesion potential.**

(A) Diploid cells have a higher volume than haploid cells. The experiment shown is a representative experiment of 4 replicates. Total of 246 haploid and 232 diploid cells were measured ( $p=7.2 \times 10^{-13}$ ). Related to Fig. 5B,C. (B) Example cell tracks of aggregating *Dictyostelium* cells within a single field of view (relates to Fig. 5D-F). High Rad51-Neon cell tracks are marked in green and low expressers in blue, with the initial position marked as a dot in the same colour and the track endpoint marked as a black dot. Scale bar 100  $\mu\text{m}$ . (C) Heatmap showing correlations between *rad51* expression and genes with GO-annotated roles in adhesion and an associated adhesion phenotype. Correlation values are taken from single cell transcriptomics data of *Dictyostelium* mounds at 14 h of development (Antolovic et al., 2019). The black rectangle highlights the correlations with *rad51*.

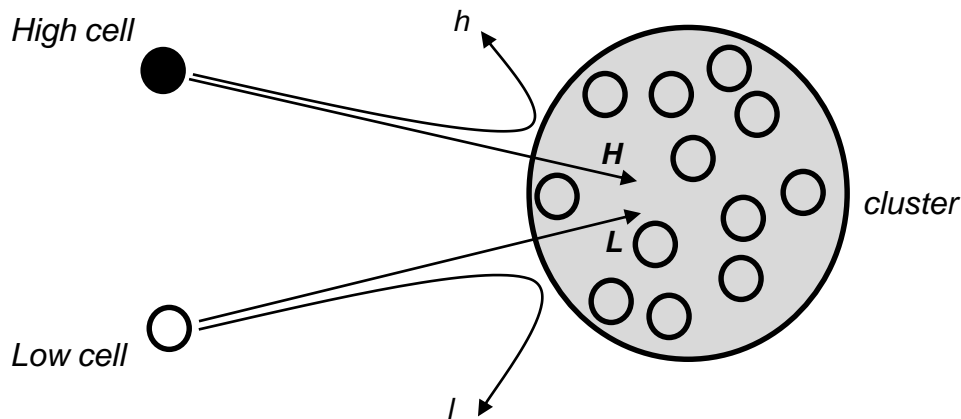


**Fig. S7. Estimation of the relative likelihood of damaged and non-damaged cells to remain non-adherent during cell cohesion assays.**

Let the number of high and low cells entering a cluster be  $H$  and  $L$ , respectively. Let the number of high and low cells rejected from a cluster be  $h$  and  $l$ , respectively. The probability that a high cell will be rejected from a cluster is  $P_h = \frac{h}{h+H}$  and the probability that a low cell will be rejected from a cluster is  $P_l = \frac{l}{l+L}$ . The relative probabilities of high and low cells being rejected from a cluster are therefore:  $\frac{P_h}{P_l} = \frac{h}{l} \times \frac{l+L}{h+H}$ . In our case  $\frac{l+L}{h+H} = 99$ . In the presence of divalent cations  $\frac{h}{l} \approx \frac{5}{95}$ , therefore  $\frac{P_h}{P_l} \approx 5.2$ . In the absence of divalent cations  $\frac{h}{l} \approx \frac{1}{99}$ , therefore  $\frac{P_h}{P_l} \approx 1$ .

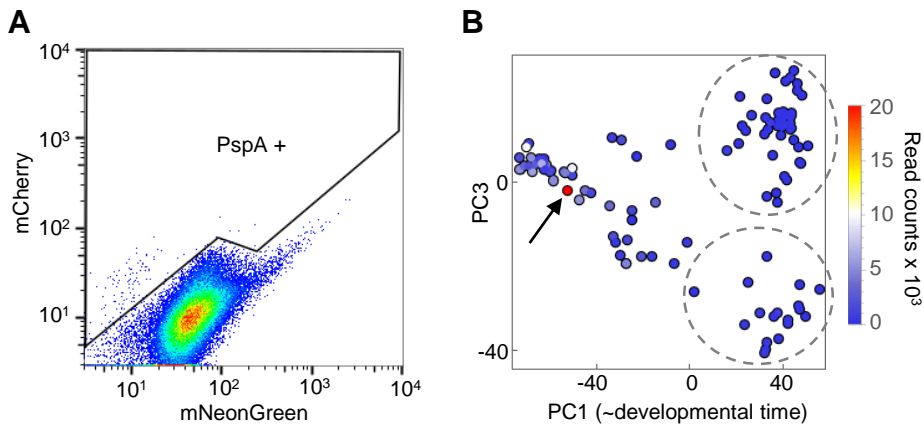


### Fig. S8. Developmental gene expression of high *rad51* cells.

(A) Setting the threshold for calling *pspA*-mCherry expression. Data show a flow cytometry plot of the Rad51-Neon cell line. The data are the same as in Fig. 6C, but overlaid with a line demarcating the specified cut off. Different selected thresholds did not alter the conclusion that high Rad51-Neon cells poorly induce mCherry from this prespore promoter. (B) Principal component analysis of single cell transcriptomic data from *Dictyostelium* mounds (Antolovic et al., 2019) coloured to show single cell levels of *rad51* mRNA. PC1 is a proxy for developmental time, with cells on the right more advanced in development. At least one cell (arrow) showed expression comparable to the undifferentiated high *rad51* cells, and this cell clustered with cells that have not showed selection of the spore (top cluster circled) or stalk fates (bottom circled cluster). These data imply that high *rad51* cells, in addition to becoming aggregation competent, can advance their gene expression at least to a state just prior to overt fate selection.

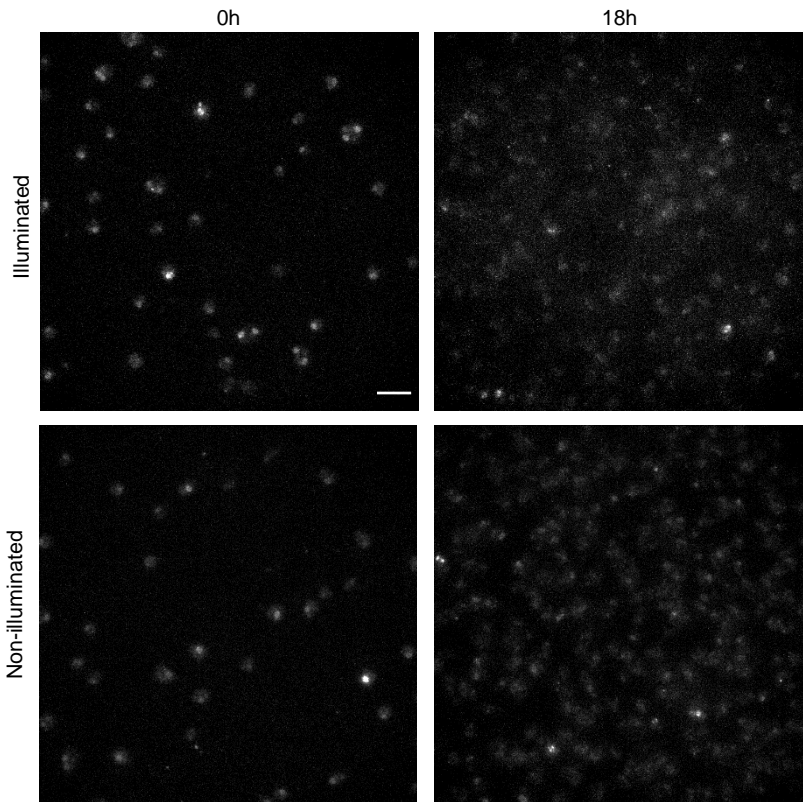


**Fig. S9. Standard imaging protocols do not induce Rad51-Neon expression.**

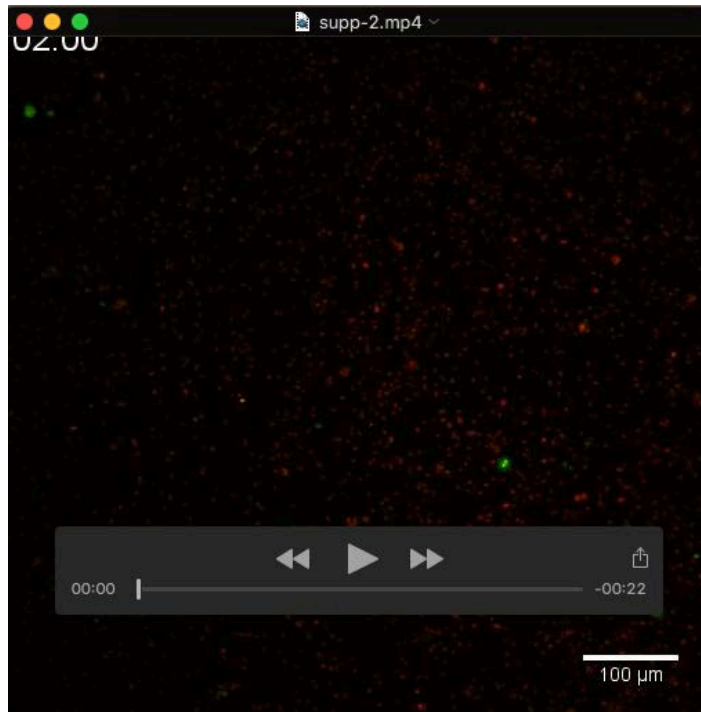
Panels show images of fields captured on the wide field imaging set up used for the cell cycle phase analysis. The images show a field of view at the onset and end of an 18 h 3D time lapse with a frame interval of 2 min, and 20 z slices per field of view per time interval. The distribution of Rad51-Neon intensities is the same for samples illuminated using this protocol, and those for which the above images were the only ones captured. Scale bar 20  $\mu$ m.

**Table S1.** Genes highly correlated in their expression to *rad51*. We searched for genes with a read out in the single cell transcriptomics of greater than 10 that had a correlation value,  $r$ , greater than 0.5. Of the 30 genes passing this cut-off, 26 are involved in DNA repair and/or replication.

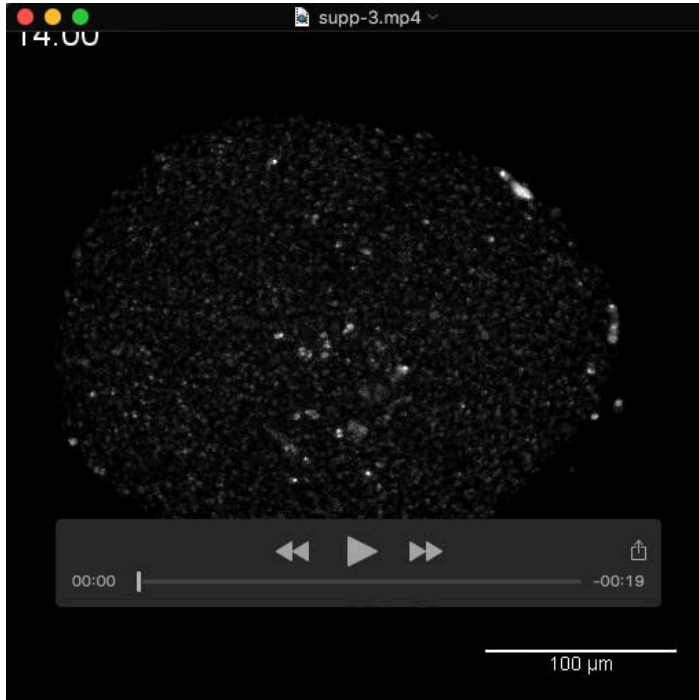
[Click here to Download Table S1](#)



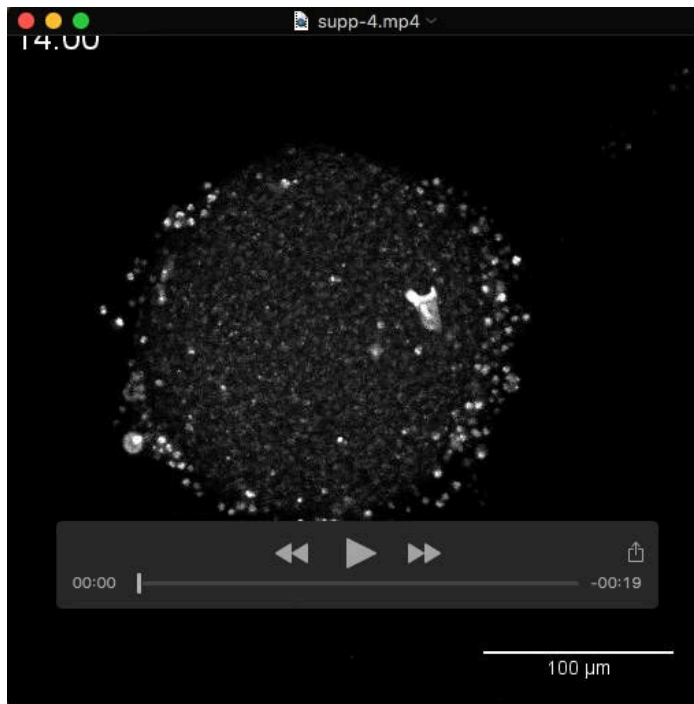
**Movie 1.** Time-lapse imaging of *Dictyostelium* aggregation showing the behaviour of cells with spontaneous DNA damage. High Rad51-Neon expressing cells can be tracked from the onset of differentiation, until late aggregation and slug departure. The high Rad51 cells appear to remain at the edge of cell aggregates. All cells express the red nuclear marker (H2Bv3-mCherry). Time after starvation onset is shown.



**Movie 2.** Time-lapse imaging of *Dictyostelium* aggregation showing the behaviour of cells with spontaneous DNA damage. Alternative movie to Movie 1. Time after starvation onset is shown.



**Movie 3.** Movie showing shedding of high Rad51 cells as an aggregate begins to move away as a slug. Time after starvation onset is shown.



**Movie 4.** Movie showing shedding of high Rad51 cells as an aggregate begins to move away as a slug. Alternative movie to Movie 3. Time after starvation onset is shown.